



HAL
open science

Water-induced crystallization and nano-scale spinodal decomposition of cellulose in NMMO and ionic liquid dope

Yoshiharu Nishiyama, Shirin Asaadi, Patrik Ahvenainen, Herbert Sixta

► **To cite this version:**

Yoshiharu Nishiyama, Shirin Asaadi, Patrik Ahvenainen, Herbert Sixta. Water-induced crystallization and nano-scale spinodal decomposition of cellulose in NMMO and ionic liquid dope. *Cellulose*, 2019, 26 (1), pp.281-289. 10.1007/s10570-018-2148-x . hal-02390952

HAL Id: hal-02390952

<https://hal.science/hal-02390952>

Submitted on 6 Aug 2022

HAL is a multi-disciplinary open access archive for the deposit and dissemination of scientific research documents, whether they are published or not. The documents may come from teaching and research institutions in France or abroad, or from public or private research centers.

L'archive ouverte pluridisciplinaire **HAL**, est destinée au dépôt et à la diffusion de documents scientifiques de niveau recherche, publiés ou non, émanant des établissements d'enseignement et de recherche français ou étrangers, des laboratoires publics ou privés.

1 **Water-induced crystallization and nano-scale**
2 **spinodal decomposition of cellulose in NMMO**
3 **and ionic liquid dope**

4 Yoshiharu Nishiyama^{1*}, Shirin Asaadi², Patrik Ahvenainen³, and Herbert Sixta²

5 ¹ *Univ. Grenoble Alpes, CNRS, CERMAV, 38000 Grenoble, France*

6 ² *Department of Bioproducts and Biosystems, Aalto University, P.O. Box 16300,*
7 *Vuorimiehentie 1, Espoo, FI-00076, Finland*

8 ³ *Department of Physics, University of Helsinki, P.O. Box 64, FI-00014,*
9 *Finland*

10 Phone: +33 (0) 476 03 76 05

11 E-mail: yoshi@cermav.cnrs.fr

12 We followed the cellulose structure formation induced by water diffusion into Lyocell dopes based
13 on both N-Methylmorpholine N-oxide (NMMO) and 1,5-diazabicyclo[4.3.0]non-5-ene acetate
14 ([DBNH][OAc], by using scanning simultaneous small- and wide-angle scattering (SAXS-WAXS)
15 experiment along the diffusion gradient. The water content at each point was estimated from the
16 wide-angle scattering profile, giving a binary diffusion constant of the order of 5×10^{-10} m²/sec. In
17 the case of the cellulose solution in NMMO monohydrate, diffraction peaks corresponding to
18 cellulose II appeared concomitantly with the increase in small angle scattering features indicative
19 of nanofibril formation. In the cellulose solution in the ionic liquid, an increase in small angle
20 scattering intensity with the progression of water content appeared at scattering vector $q = 0.015$
21 \AA^{-1} corresponding to a correlation length of about 40 nm, indicative of nanometric spinodal
22 decomposition preceding the coagulation process, though no crystalline peak appeared in the wide-
23 angle scattering.

24

25 *SAXS-WAXS, dissolution, regeneration, coagulation, diffusion, ionic liquid*

26

27 Introduction

28 Structure formation during the processing from highly concentrated solution dope is a crucial step
29 in controlling the final material properties in solution processing, including fiber spinning,
30 membrane generation or fabrication of other functional materials. One of the reasons for the
31 success of viscose process for the manufacture of regenerated cellulose fibers, despite its
32 environmental concerns, is its ability to adjust various fiber properties and supramolecular
33 structures by modifying the operational conditions. For other potential solvent systems that can be
34 more environmentally benign to be deployed more massively, the control of the structural
35 formation is a key. However, little is known on the structure formation process at nanoscale.
36 NMMO is a solvent used in the industrial production of cellulose fibers called Lyocell while
37 [DBNH][OAc] is a new ionic solvent that has promising characteristics as next generation solvent
38 for cellulose processing (Sixta2015). Both are miscible with water but lose their cellulose
39 dissolution capacity with excess water. Thus water is used as non-solvent to regenerate cellulose.
40 In the spinning process, the humidity in the air gap is known to be an important parameter
41 (Mortimer1996), but its role remains hypothetical in the absence of experimental data on the
42 structure modification.

43 The regeneration of cellulose by a non-solvent, in this case water, is a complex process involving
44 diffusion of non-solvent into the dope, diffusion of different solvent molecules into coagulation
45 bath and the structure formation and swelling or contraction of the regenerating gel. Thus there is a
46 huge difference in estimated diffusion coefficients depending on the experimental approach and
47 the diffusion model employed.

48 A critical review of the literature data is available in a recent report by Hedlund et al (2017). The
49 reported value of diffusion coefficient of water and NMMO in NMMO/cellulose dope measured
50 by visual inspection of diffusion front (Biganska2005), after correction of equation as pointed out
51 by Hedlund et al (multiplication by factor of 4), was $4.4 \times 10^{-9} \text{ m}^2/\text{s}$, which is higher than the self-
52 diffusion coefficient of water at ambient conditions ($2.57 \times 10^{-9} \text{ m}^2/\text{s}$). The self-diffusion of NMMO
53 to the coagulation bath was estimated to be about one order of magnitude lower, and further
54 decreasing in the presence of cellulose (Biganska2005).

55 By using NMR diffusometry, Laity et al (2012) assessed the self-diffusion coefficient of NMMO
56 and water molecules in NMMO/cellulose solution to be of the order of $4 \times 10^{-12} \text{ m}^2/\text{s}$, which
57 increases to the order of $1.5 \times 10^{-9} \text{ m}^2/\text{s}$ in the course of coagulation with water, while effective
58 mutual diffusion during coagulation as estimated from composition change was $1.4 \times 10^{-10} \text{ m}^2/\text{s}$
59 with the NMMO loss and water influx to be identical (Laity2002). Similar NMR studies on ionic
60 liquid systems show the diffusion coefficient of pure ionic liquid (1-ethyl-3-methyl-imidazolium
61 acetate) to be $10^{-11} \text{ m}^2/\text{s}$ and this value can go down by two orders of magnitude in the presence of
62 carbohydrates due to the association with hydroxyl groups (Ries 2014). In the ionic liquid-water
63 system, the diffusion constant of ionic liquid increases under the presence of water, while that of
64 water is slowed down by the presence of an ionic liquid (Hall2012).

65 The diffusion of solvents and non-solvents during the regeneration of cellulose depend also on the
66 network structure of regenerating cellulose. Gavillon and Budtova (2007) measured decreased

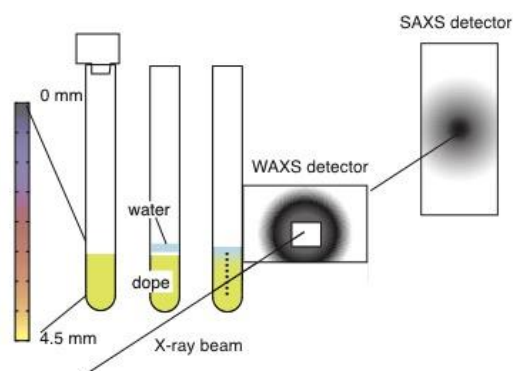
67 diffusion coefficients of NaOH and NMMO in the presence of coagulating cellulose that would
68 indicate homogeneous gel formation where individual chains would interact with the solvent.. On
69 the other hand Hedlund (2017) observed little effect of cellulose in [C2min][OAc] system
70 indicative of heterogeneous gel formation in which most of cellulose chains would be excluded
71 from the solvent system.
72 However, diffusion is also affected by many factors such as intermolecular interactions. The
73 structure of coagulating cellulose, which can also depend on the cellulose concentration, cannot be
74 directly determined from the diffusion data alone. X-ray scattering is a powerful tool to probe the
75 spatial arrangement, from sub-nanometric to sub-micrometric length scale inside a sample. In this
76 study, we measured simultaneous small- and wide-angle X-ray scattering on regenerating cellulose
77 near water (coagulant) solution interface to follow the structural formation.
78

79 **Experimental**

80 **Materials**

81 Birch pre-hydrolyzed kraft pulp (PHK) with DP 1007, $M_w = 274.3 \text{ kg mol}^{-1}$, $M_n = 68.2 \text{ kg mol}^{-1}$
82 and PDI = 4 from Stora Enso Enocell Mill, Finland was used as a cellulose solute. 1,5-
83 Diazabicyclo[4.3.0]non-5-ene (DBN) (99%, Fluorochem, UK) and glacial acetic acid (Merck,
84 Germany) were used as received. [DBNH][OAc] ionic liquid was synthesized by slowly adding
85 equimolar amounts of acetic acid to DBN under cooling (Michud 2015). The cellulose solutions
86 were prepared in a 200 ml vertical kneader rotating at 30 rpm, under a vacuum of 3 to 5 mbar. The
87 temperature was regulated to 90°C for the NMMO system and 80°C for [DBNH][OAc] system. It
88 took 90 minutes to prepare a 10 wt% cellulose solution. For the NMMO system, 0.15 to 0.28 g of
89 propyl gallate was added to the dopes as stabilizer.
90 The samples were put in a glass tube with an outer diameter of 3 mm and a wall thickness of 200
91 μm . The [DBNH][OAc] cellulose solution was viscoelastic at room temperature, and thus a hot
92 solution was centrifuged at 3000 rpm for 1 min to fill in the bottom of the tube. The cellulose-
93 NMMO dopes were solid at room temperature, and could be easily loaded into the tubes.

94 **X-ray scattering**



95

96 Figure 1. Schematic illustration of the experimental setup.

97

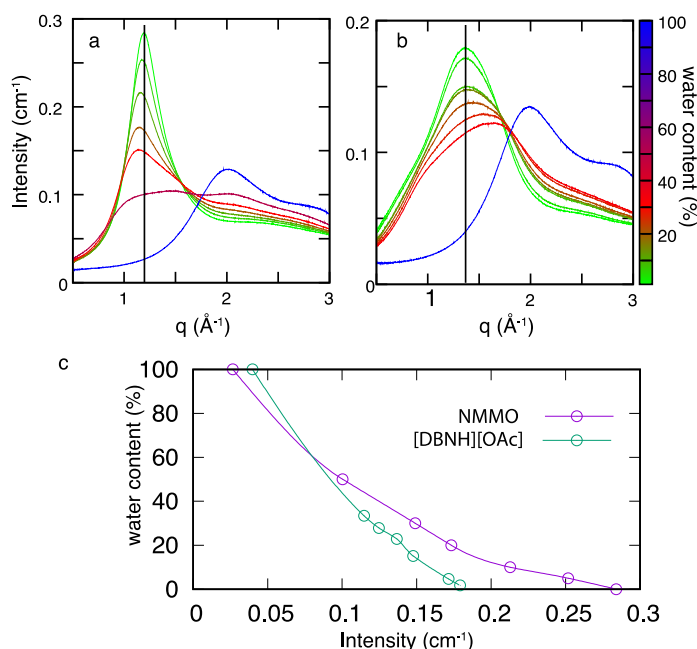
98 The X-ray scattering experiment was carried out at the D2AM beamline of the ESRF. Two silicon
99 pixel detectors were used simultaneously. A detector with central hole, "WOS" (imXPAD, France)
100 was placed at about 7 cm from the sample and a rectangular detector "XPAD-D5" (imXPAD,
101 France) was placed at 1.5 m from the sample. The sample tubes were mounted on a temperature
102 controlled sample exchanger with 3 mm diameter holes mounted on a motorized sample stage. X-
103 ray energy of 18 keV ($\lambda = 0.689 \text{ \AA}$) was chosen to limit the attenuation by the glass tube. The
104 exposure time was 10 seconds for each frame. The incident and the transmitted beam intensities
105 were monitored by scintillation counters placed before and behind the sample respectively. The
106 scattered intensity was normalized with respect to the transmitted intensity, and the scattering
107 signal from the empty glass tube was subtracted. The intensities were circularly averaged after
108 Lorentz-polarization correction using an inhouse software, and converted to differential scattering
109 cross sections [cm^{-1}] by calibrating with water scattering intensity (Dreiss2006). The scattering
110 intensities are presented as a function of the magnitude of the scattering vector

$$q = \frac{4\pi \sin \theta}{\lambda} (\text{\AA}^{-1})$$

111 where 2θ is the angle between the incident beam and the scattering direction.

112

113 Wide angle scattering of solvent and water content



114

115 Figure 2. Wide angle scattering of solvent-water mixture of (a) NMMO monohydrate at 90°C and
116 (b) [DBNH][OAc] at 80°C as a function of water content (not taking into account the initial
117 hydration of NMMO). c: Relationship between water content and the scattering intensity at 1.2 Å⁻¹

118 for NMMO monohydrate and 1.4 \AA^{-1} for [DBNH][OAc]. Data points were connected with an
119 Akima spline interpolation (solid line in the figure)

120

121 A series of X-ray scattering profiles of solvent-water mixtures measured at 80°C for
122 [DBNH][OAc] and 90°C for NMMO monohydrate are presented in figure 2. The scattering of
123 neat [DBNH][OAc] and NMMO monohydrate has maximum intensity at $q = 1.4$ and 1.2 \AA^{-1}
124 respectively whereas water scattering peaks at around 2 \AA^{-1} . With increasing water content, the
125 scattering profile continuously changes and each mixture has a unique profile. The relation
126 between water content and intensity at these peak positions are plotted in figure 2c, where a
127 reasonable estimate of water content can be obtained from the single intensity value. An Akima
128 spline (Akima1970) was used to relate the intensity to the water content. In the case of cellulose
129 dope, the presence of cellulose would slightly modify the wide angle scattering, but this effect was
130 neglected as a first approximation.

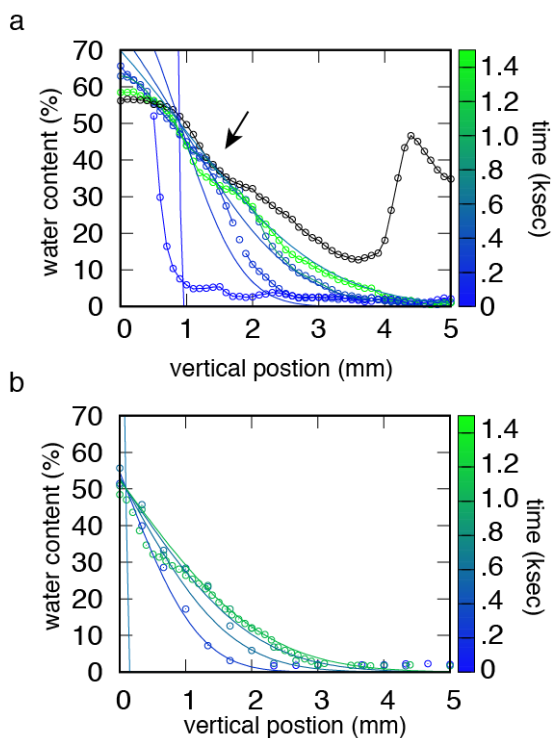
131

132 **In-situ monitoring of coagulation**

133 To follow the coagulation process with contact to water, the sample was filled to approximately 5
134 mm from the bottom of the tube, mounted on the temperature controlled sample holder, and a
135 water drop (ambient temperature) was inserted from the top to allow diffusion into the solution.
136 The temperature was maintained at 80°C for the [DBNH][OAc] system and 90°C for the NMMO
137 system. The sample was vertically scanned before and after addition of water and with regular
138 interval to monitor the structural evolution.

139 **Results and discussions**

140 **Water diffusion from wide angle scattering**



141

142 Figure 3. Water contents as function of position during regeneration from (a) NMMO and (b)
 143 [DBNH][OAc] as calculated from the scattering intensity at $q = 1.2 \text{ \AA}^{-1}$ for NMMO and $q = 1.4 \text{ \AA}^{-1}$
 144 for [DBNH][OAc] according to Fig 2c. The black curve in (a) is obtained after cooling at room
 145 temperature. The apparent steps in (a) are probably an artifact due to the crystallization as seen in
 146 figure 4.

147

148 When water is added the wide-angle scattering feature reproduces the scattering features of water-
 149 NMMO mixture and water-[DBNH][OAc] mixture with increasing concentration of water towards
 150 the top of the tube. The water content estimated from the scattering intensity at $q = 1.2 \text{ \AA}^{-1}$ and at q
 151 $= 1.4 \text{ \AA}^{-1}$ according to Fig 2c as a function of vertical position is plotted in figure 3. For a Fickian
 152 diffusion with a constant diffusion constant D , the water content C at position x from the interface,
 153 after time t since the contact with water can be expressed as (Crank1975)

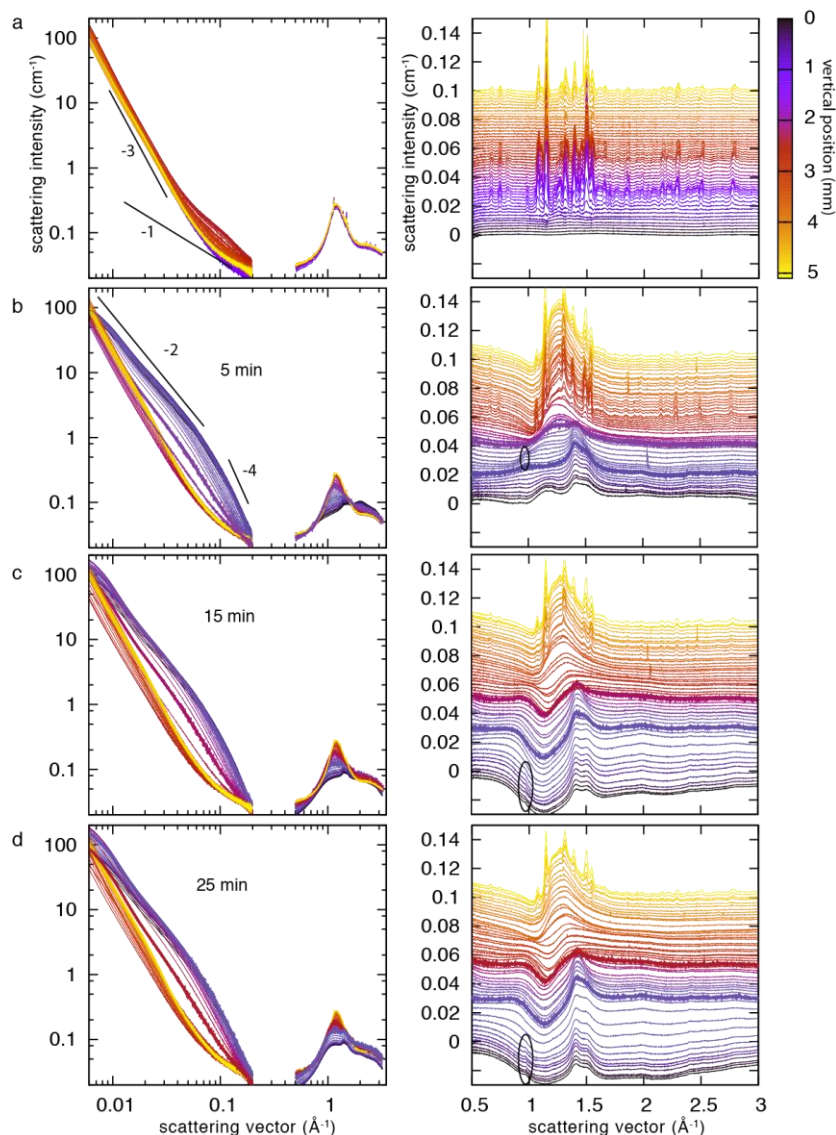
$$C(x, t) = \text{erfc} (x/(4tD)^{1/2})$$

154 This prediction of concentration distribution is overlapped as solid line on the concentration
 155 evaluated from the scattering intensity. Here, in both cases, a mutual diffusion constant of 5×10^{-9}
 156 m^2/s was used. Since the volume beneath the vertical reference position is held constant by the
 157 tube wall, the influx of water into the solution is equal to the solvent and cellulose outflux from
 158 vertical position 0. The self-diffusion coefficient of water at 80°C is $6.25 \times 10^{-9} \text{ m}^2/\text{s}$ (Yoshida2008)
 159 so the apparent diffusion coefficient is not far from the pure water, contrary to what was estimated

160 from NMR diffusometry. In some places the water diffusion seems to be even faster (arrow in fig.
161 3) which might be due to the presence of microcavities.

162

163 Regeneration from NMMO solution



164

165 Figure 4 a-d: Small- and wide-angle X-ray scattering profiles of 10% cellulose dope in NMMO
166 monohydrate as a function of vertical position along the tube (color code) at 90°C before addition
167 of water (a) and 5 min (b), 15 min (c) and 25 min (d) after addition of water. The left figures are
168 double logarithmic plots of data covering both wide- and small angle scattering data, and the right
169 figures are linear scale plots after subtraction of solvent/water mixture profile obtained by
170 interpolation of experimental data in Figure 2, with water content estimated from the scattering
171 intensity at $q = 1.2 \text{ \AA}^{-1}$ according to figure 2c. The profiles at the transition when the peak
172 appears at $q = 1.4$ and 1.5 \AA^{-1} are drawn with thicker lines for clarity. Power law lines with
173 different exponents are indicated as guides to the eye.

174

175 Before the addition of water, the small-angle scattering of cellulose solution in NMMO
176 monohydrate at 90°C followed a power law with an exponent of -3 below $q = 0.08 \text{ \AA}^{-1}$, steeper
177 than what would be expected for an extended polymer chain segments. This excess scattering
178 intensity below $q = 0.08 \text{ \AA}^{-1}$ indicates heterogeneity of the solution structure or density fluctuations
179 at least at a nanometric length scale. In the wide-angle range, depending on the position of the
180 beam, sharp crystalline peaks can be seen (figure 4a right). On the other hand the feature in the
181 small angle region below $q = 0.04 \text{ \AA}^{-1}$ is independent of position, and thus should not be related to
182 the crystallization seen in the wide-angle scattering that is more heterogeneous and localized. One
183 possibility would be micro cavities with irregular surfaces or polydisperse nanobubbles created
184 during the crystallization of NMMO when the solution was cooled down. In theory, the high
185 surface tension could lead to rapid Ostwald ripening. The kinetics of Ostwald ripening also
186 depends on the volume fraction of bubbles and the solubility of the gas, which can be small. The
187 intensity increase at low q can also be due to the aggregation of cellulose chains. In this case, it
188 would be a loose association of cellulose chains as there is no sign of cellulose crystallinity in the
189 wide-angle scattering. Some positions show a shoulder appearing at around $q = 0.1 \text{ \AA}^{-1}$, which
190 again does not correlate with crystalline peak intensity. For the moment we do not have any
191 explanation for this feature.

192 In the small-angle region, about five minutes after the addition of water (Fig. 4b), the scattering
193 intensity in the q -range of $0.01 - 0.02 \text{ \AA}^{-1}$ increases at positions close to the water interface, up to
194 vertical position of 2 mm, due to a coarse structuring (thick line in fig 4b). On the other hand, the
195 intensity decreased in lower positions with diffusion of water. This decrease can be explained if
196 the scattering from the dope originated from microcavities that are now filled with water in the
197 first place, thus reducing the electron density contrast between the cavity and the bulk.

198 The first increase in intensity from the original profile can be seen between $q = 0.03 - 0.1 \text{ \AA}^{-1}$ at a
199 position 2 mm from the top, corresponding to about 10 wt-% water content (not counting the
200 hydration molecule of the monohydrate). The exact peak position of the new signal cannot be
201 determined due to the uncertainty of the high scattering coming from the coarse structure that exist
202 already before addition of water.

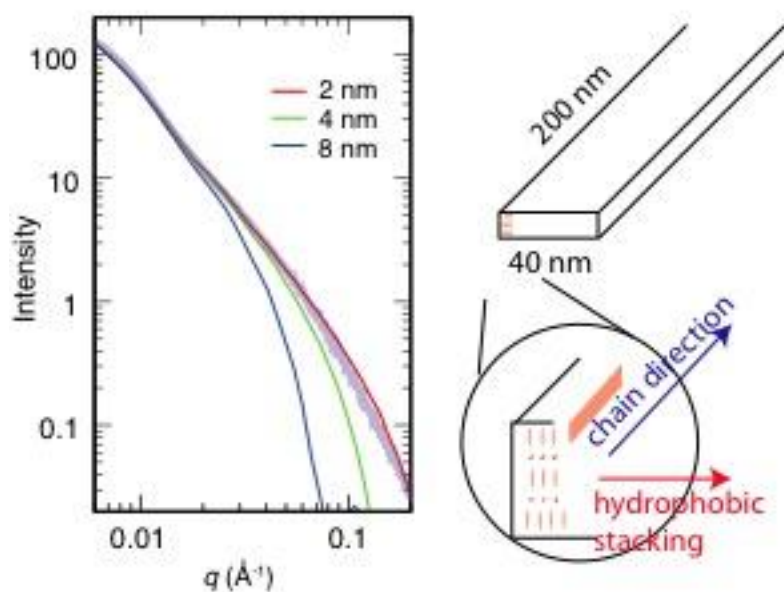
203 In the wide-angle range, the sharp diffraction disappears at water content of about 5% (vertical
204 position = 2.5 mm), and a crystalline peak typical of polymer crystals starts to appear at the
205 vertical position of 2 mm, corresponding to a water content of 10%, first at $q = 1.4 \text{ \AA}^{-1}$ followed by
206 another peak at $q = 1.5 \text{ \AA}^{-1}$ further closer to the interface (v. p. = 1.8 mm, water content =15%,
207 drawn with thick line in fig. 4b). These peaks corresponds to a d -spacings of 4.5 and 4.2 \AA
208 respectively which is close to the strongest reflections of cellulose II, 1 1 0 and 0 2 0 ($d = 4.4$ and
209 4.0 \AA), and is probably due to the crystallization of cellulose essentially in the direction
210 perpendicular to the pyranose plane, and not completely in form of cellulose II, as the peak
211 positions are slightly different and 1-10 cannot be seen. The two peaks are also quite similar to Na-
212 cellulose complex (Nishiyama2000), and might be due to a similar loose complex structure
213 involving NMMO molecules. The very early stage of coagulation showing only one peak at $d =$
214 4.5 \AA is also reported by Fink et al (2001) in the never-dried fiber from the NMMO system. In our

215 condition the crystalline order grew perpendicular to the hydrophobic stacking as well, though to a
216 smaller size than in the hydrophobic stacking direction.

217 The scans at 15 and 25 minutes after the introduction of water (Fig. 4c, d) capture the progression
218 of water diffusion and the accompanying structure formation. In both cases, the change in small-
219 angle scattering features coincided with the appearance of the first diffraction peak at $q = 1.4 \text{ \AA}^{-1}$,
220 indicating that the structuration is essentially due to crystallization, or stacking of chains in one
221 direction occurring at relatively low water content of 10%.

222 Some aspects seem to be governed by timescale accessible in this experiment ~ minutes. For
223 example, a small peak at 0.97 \AA^{-1} corresponding to $d = 6.5 \text{ \AA}$ first appears after 5 min in the zone
224 where water content is 30-40%, but disappears from this zone in the later stages, reappearing in the
225 zone closer to the water interface. The current data do not allow a clear molecular view of the
226 structure formation, but the distance would be compatible with molecular distances in the plane
227 parallel to pyranose plane.

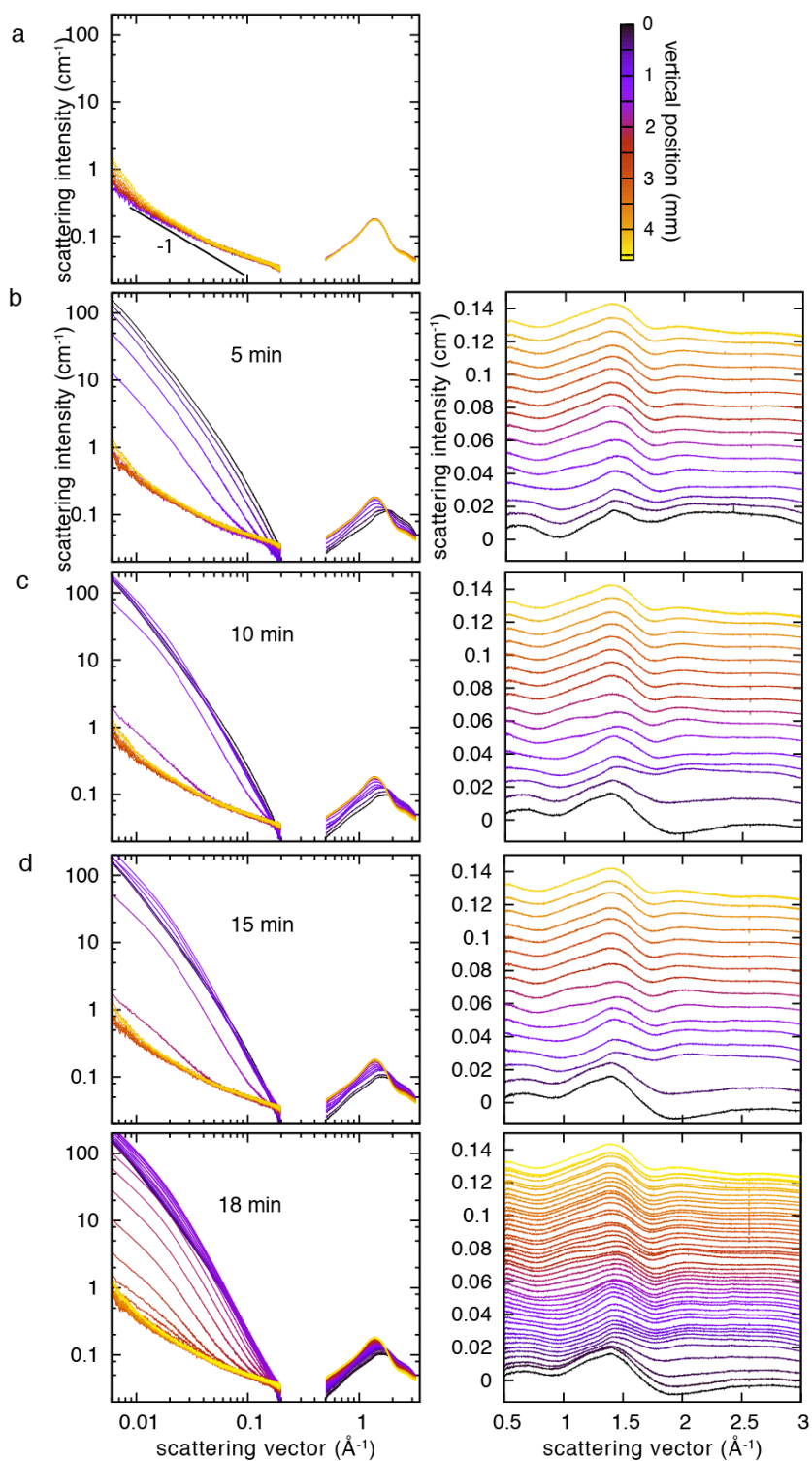
228 The slope of the small angle scattering between $q = 0.1$ and 0.2 \AA^{-1} is close to -4 and is compatible
229 with formation of nanometric crystalline fibrils that make clear boundaries between the solvent,
230 Between $q=0.01$ and 0.06 \AA^{-1} , the slope is close to -2, typical of a flat object. The diffraction
231 features suggested that the crystallization to be very directional, perpendicular to the pyranose
232 plane, which agrees with the vision of a flat ribbon to be formed. For comparison, figure 5 shows a
233 simulated scattering profile for a randomly oriented cuboid 200 nm long, 40 nm wide and with
234 thickness ranging from 2 to 8 nm, which show general agreement with the scattering profile,
235 especially when the thickness was 2 nm. A thickness of 2 nm could correspond to about three
236 layers of cellulose sheets intercalating NMMO and water molecules. At q above 0.2 \AA^{-1} , the
237 simulation deviates from the observation, as the coagulated object cannot be considered as
238 homogeneous cuboid at this length scale giving rise to excess scattering in the real world. Of
239 course this is not the only model that can explain the small small-angle scattering profile and it
240 should be considered as one of the plausible models.



241

242 Figure 5. Simulated scattering profile (left) of cuboid presented on the right with different
243 thicknesses (2, 4, 8 nm) overlapped with the experimental data from Fig 4d (thick lines) showing
244 good agreement with the 2 nm thick model .

245 Regeneration from [DBNH][OAc] solution



246

247 Figure 6. Small- and wide-angle X-ray scattering profiles of 10% cellulose dope in [DBNH][OAc]
248 as a function of vertical position along the tube (color code) at 80°C before addition of water (a)
249 and 5 min (b), 10 min (c) 15 min (d) and 18 min (e) after the addition of water

250

251 X-ray scattering profiles of 10% cellulose solution in [DBNH][OAc] at 80°C is shown in figure 6a.
252 Contrary to NMMO solution, there is no indication of a coarse structure or density fluctuation
253 except for slight excess intensity at lowest $q \sim 0.01 \text{ \AA}^{-1}$ in some parts of the sample. The intensity
254 follows $I \sim q^{-1}$ with a prefactor similar to the case of cellulose solution in NMMO monohydrate,
255 typical of a rod-like scattering object.

256 When water is added, the intensity drastically rises below $q = 0.1 \text{ \AA}^{-1}$ forming concave upward
257 profiles, even with the slightest change in the wide-angle scattering. Throughout the experiment no
258 crystalline peak appeared in the wide-angle scattering. The first event of regeneration is the density
259 fluctuation, probably induced by the spinodal decomposition. This is different from the case of
260 regeneration from NMMO solution where elongated plate-like crystalline domain forms. The
261 regeneration event starts with an appearance of a small shoulder peak in the small angle region
262 between 0.01 and 0.02 \AA^{-1} corresponding to a density fluctuation with a periodicity of 30-60 nm.
263 The increase in small angle intensity occurs at water content of about 5% and completes below
264 15% water content, the transition corresponding to a depth at about $500 \mu\text{m}$ as judged from the
265 wide-angle scattering according to figure 2.

266 The spun fibers from [DBNH][OAc] are known to be crystalline, similar to the NMMO-based
267 Lyocell fibers (Sixta2015, Hummel 2016). In this simple experiment, no extensional flow or shear
268 that would force the alignment of cellulose chains exists. In the spinning process, such strain can
269 facilitate the crystallization. Also, the water content at the interface was only 50%, and still the
270 cations can be strongly bound to the cellulose chains impeding the crystallization. The
271 crystallization in the process might be occurring during the washing stage where the solvent
272 concentration is much lower. Indeed the particularity of the [DBNH][OAc] is the apparent slow
273 diffusion from cellulose gel (Hauru2016) that might be due to strong affinity to cellulose. These
274 points will be investigated in the future by analyzing further the washing stage, and the effect of
275 different strain conditions on the sample during the regeneration.

276 Conclusion

277 A simultaneous wide- and small-angle X-ray scattering allowed us to follow the water diffusion
278 during regeneration, crystallization behavior and nano-structure formation of cellulose during
279 regeneration process. Unidirectional crystallization was the first step of coagulation in the NMMO
280 dope /water regeneration, while no crystallization was observed in the regeneration process of
281 [DBNH][OAc], up to a water content of approximately 50%.

282

283 Acknowledgements

284 We thank Dr. Isabelle Morfin, Dr. Nathalie Boudet and Dr. Nils Blanc for assistance at the
285 D2AM beamline, and ESRF for providing beamtimes. PA has received funding from Kone
286 Foundation.

287

288

289 References

- 290 Akima H (1970) A new method of interpolation and smooth curve fitting based on local
291 procedures. *J.ACM* 17, 589-602.
- 292 Biganska O, Navard P (2005) Kinetics of precipitation of cellulose from cellulose – NMMO –
293 water solutions. *Biomacromol.* 6, 1948-1953.
- 294 Crank J (1975) *The mathematics of diffusion*. second ed. Clarendon Press, Oxford p.14
- 295 Dreiss CA, Jack KS, Parker AP. (2006) On the absolute calibration of bench-top small-angle X-ray
296 scattering instruments: a comparison of different standard methods. *J. Appl. Cryst.* 39, 32-39.
- 297 Fink HP, Weigel P, Purz HJ, Ganster J. (2001) Structure formation of regenerated cellulose
298 materials from NMMO-solutions. *Prog. Polym. Sci.* 26, 1473-1524.
- 299 Hall CA, Le KA, Rudaz C, Radhi A, Lovell CS., Damion RA., Budtova T, and Ries ME (2012)
300 Macroscopic and microscopic study of 1- ethyl-3-methyl-imidazolium acetate–water mixtures. *J.*
301 *Phys. Chem B* 116, 12810–12818.
- 302 Hauru LKJ, Hummel M, Nieminen K, Michud A, Sixta H (2016) Cellulose regeneration and
303 spinnability from ionic liquids. *Soft Matter* 12, 1487-1495.
- 304 Hedlund A, Könke T, Theliander H (2017) Diffusion of ionic liquid – cellulose solutions during
305 coagulation in water: mass transport and coagulation rate measurements. *Macromolecules* 50,
306 8707–8719.
- 307 Hummel M, Michud A, Tantt M, Asaadi S, Ma Y, Hauru LKJ, Parviainen A, King AWT,
308 Kilpeläinen I, Sixta H (2016) Ionic liquids for the production of man-made cellulosic fibers -
309 opportunities and challenges. *Adv. in Polym. Sci.* 271, 133-168.
- 310 Laity PR, Glover PM, Hay JN (2002) Composition and phase changes observed by magnetic
311 resonance imaging during non-solvent induced coagulation of cellulose. *Polymer* 43, 5827-5837.
- 312 Liu R and Hu X (2006) Precipitation kinetics of cellulose in the Lyocell Spinning Process. *Ind.*
313 *Eng. Chem. Res.* 45, 2840-2844.
- 314 Michud A, Tantt M, Asaadi S, Ma Y, Netti E, Käärläinen P, Persson A, Berntsson A, Hummel M
315 Sixta H (2015) Ioncell-F: ionic liquid-based cellulosic textile fibers as an alternative to viscose and
316 Lyocell. *Textile Res. J.* 86, 543-552
- 317 Mortimar SA and Peguy A (1996) The influence of air-gap conditions on the structure formation
318 of lyocell fibers. *J. Appl. Polym. Sci.* 60, 1747-1756.
- 319 Nishiyama Y, Kuga S, Okano T (2000) Mechanism of mercerization revealed by X-ray diffraction.
320 *J. Wood Sci.* 46, 452-457.
- 321 Sixta H, Michud A, Hauru L, Asaadi S, Ma Y, King AWT, Kiplenäinen I, Hummel M (2015)
322 Ioncell-F: A High-strength regenerated cellulose fibre. *Nordic Pulp & Paper Res. J.* 30, 43-57.

323 Yoshida K, Matubayasi N, Nakahara M (2008) Self-diffusion coefficients of water and organic
324 solvents at high temperatures along the coexistence curve J. Chem. Phys. 129, 214501
325